Dalton Transactions

Accepted Manuscript

Journal Name RSCPublishing

ARTICLE

Multifunctional MOFs through CO_2 fixation: a metamagnetic kagome lattice with uniaxial zero thermal expansion and reversible guest sorption

Cite this: DOI: 10.1039/x0xx00000x

Received 00th January 2012,
Accepted 00th January 2012

DOI: 10.1039/x0xx00000x

www.rsc.org/

Tony D. Keene,[a,b] Michael J. Murphy,[b] Jason R. Price,[b,c] Natasha F. Sciortino,[b] Peter D. Southon[b] and Cameron J. Kepert*[b]

The properties of atmospheric CO_2 fixation, metamagnetism, reversible guest adsorption and zero thermal expansion have been combined in a single robust MOF, $[Cu_3(bpac)_3(CO_3)_2](ClO_4)_2\cdot H_2O$ (**1**·H_2O). This compound is a ditopically-bridged copper carbonate kagome lattice where desolvation of the MOF allows subtle tuning of the metamagnetic and uniaxial ZTE behaviour.

Introduction

The past decade has seen the rapid expansion of the field of metal-organic frameworks (MOFs) as functional materials capable of advanced chemical and physical function, such as host-guest, magnetic, electronic and optical properties amongst many others.[1] Advances over these traditionally disparate areas can be attributed in large measure to the intricate control conferred by the metallo-supramolecular approach to materials design, in which the rational assembly of molecular building units leads to a high degree of control over materials structure and resulting function. In addition to allowing the targeting of individual properties of interest, this approach usefully allows the strategic design of systems in which multiple properties coexist. Multifunctional materials achieved through this route are of interest in offering the ability to perturb and therefore systematically examine individual properties of interest. Moreover, the interplay between multiple properties can in some cases lead to new materials phenomena, as seen for example in the novel host-guest chemistry of electronically bistable MOFs.[2]

One field in which MOFs have generated particular interest is that of their use in carbon capture and utilisation.[3] Current solution-based adsorption processes for carbon capture are energy-intensive and use solutions of corrosive amines that can be difficult to handle effectively.[4] In one recent development, MOFs containing pendant amines have been shown to adsorb CO_2 highly selectively through carbamate formation.[5] Such an approach is an extension of the Solvay process, which uses ammonia in brine to fix CO_2 as hydrogencarbonate.[6] In parallel developments, similar chemical approaches involving the generation of organic and inorganic carbonates are being applied to large-scale CO_2 utilisation.[7]

Another interesting and potentially useful functionality of MOFs emerges from their anomalous thermomechanical behaviour.[8] Many vibrationally flexible framework materials show negative thermal expansion, decreasing in volume on heating through population of transverse vibrational modes in the framework linkages that draw together metal centers, most notably those of cyanide-bridged materials[9] and arylcarboxylates.[10] Zero- and negative thermal expansion (ZTE and NTE) materials are of considerable interest for use in precision components where thermal expansion has a deleterious effect on the performance of devices.

The coexistence of porosity and molecular magnetism is rather less intrinsic due to the somewhat competing requirements of open framework architectures and short magnetic exchange pathways. Despite the seeming exclusivity of these properties, rapid advances have been made in recent years following the establishment of synthetic design principles, leading to a powerful new route for exploring magnetic structure-property relationships.[11]

Here we report the combination of these properties – atmospheric CO_2 fixation, zero thermal expansion and molecular magnetism, along with a single-crystal to single-crystal transformation – in a single multifunctional open-framework MOF, $[Cu_3(bpac)_3(CO_3)_2](ClO_4)_2\cdot H_2O$, **1**·$H_2O$ (where bpac is 4,4′-bipyridylacetylene). The synthesis, structure, thermal behaviour and magnetic properties of this compound are presented.

Results and Discussion

Monophasic single crystal samples of **1**·H_2O were obtained through a modified Solvay process where CO_2 is adsorbed from the air and fixed in solution by ammonia solution as hydrogencarbonate. Subsequent evolution of the ammonia with evaporation allows the copper ions to be chelated by the carbonate. The structure of **1**·H_2O[12] (figure 1) consists of $[Cu_3(CO_3)_2]^{2+}$ kagome layers in the *ab*-plane bridged by bpac through the Cu(II) centres in the *c*-axis. The Jahn-Teller axes of the Cu(II) centres lie in the plane of the kagome layer, leading to a concerted rotation of each carbonate unit from its regular orientation by 15.73° (Cu1−O1 = 1.995(3) Å, Cu1−O1′ = 2.649(3) Å). Disordered ClO_4^- anions reside both in the hexagonal pores of the kagome layer and in the voids between the bpac alkyne groups, with disordered water molecules lying in the pore space between these (a full structural description can be found in the ESI).

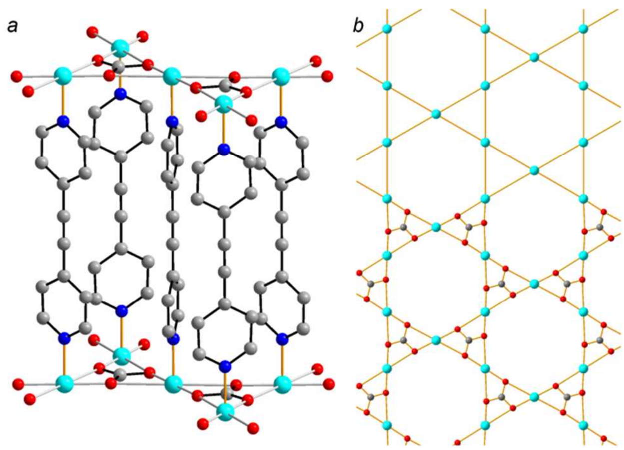

Figure 1. a) Section of the pillared kagome lattice in **1**·H_2O with disordered perchlorate and water removed for clarity; b) the kagome lattice in **1**·H_2O.

Thermogravimetry of **1**·H_2O revealed a gradual loss of the solvent water below 110 °C (figures S2 and S3, ESI). The water adsorption isotherm for **1** (figure 2) shows reversible and near-stoichiometric adsorption of water by the dehydrated material, indicating the robust nanoporosity of **1**.

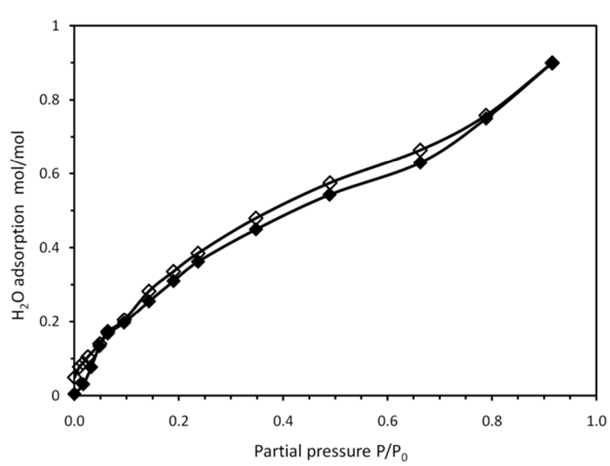

Figure 2. Water adsorption isotherm for **1** at 25°C. Unfilled data points indicate the desorption scan.

In-situ variable temperature single crystal X-ray measurements show that the guest water evolution occurs *via* a single-crystal to single-crystal transformation to form the apohost **1**, for which careful analysis found no residual electron density at the position formerly occupied by the water molecule.[13] The framework is highly stable to guest desorption, with minimal changes in the framework geometry including a very subtle contraction of 1.4% in unit cell volume, 0.5% in *a* and 0.3% in *c* when **1**·H_2O and **1** are compared at 150 K. In the desolvated material, a small pore volume of roughly 26 Å^3 is found in the space formerly occupied by H_2O, but only if the probe radius for assessing the pore volume is reduced to 1.0 Å, smaller than the van der Waal's radius of water indicating contraction of the cell on desolvation.

Unit cell collections between 100-400-175 K (figure 3) show uniaxial ZTE in the *c*-axis in **1**·H_2O with $\alpha_c = -0.2(4) \times 10^{-6}$ K^{-1} for the range 100−275 K (where $\alpha_x = dx/xdT$) and NTE in **1** with $\alpha_c = -5.4(2) \times 10^{-6}$ K^{-1} for the range 400−175 K. In both **1**·H_2O and **1**, a large positive thermal expansion (PTE) is seen in *a* and *V* with coefficients of +45.1(7) and +90.4(16) × 10^{-6} K^{-1}, respectively, for **1**·H_2O and +45.8(7) and +86.6(14) × 10^{-6} K^{-1}, respectively, for **1**. We ascribe the ZTE in the *c*-axis of **1**·H_2O to the balancing of two opposing influences: bond length expansion associated with longitudinal vibrations (favouring PTE) and pronounced transverse motion of the bpac ligand (favouring NTE). This is the first time, to our knowledge, that a nitrogen-donor ligand has led to anomalous thermal expansion behaviour. The expansion coefficients are remarkably similar in the solvated and desolvated forms of this compound, with the conversion from ZTE to weak NTE along *c* being attributable to the increased amplitudes of transverse vibration of the bpac unit with removal of the pore water guests.[14] The presence of these guests near the bpac ethyne group in the solvated form therefore appears to play an important role in fine-tuning the ZTE behaviour through dampening the transverse bpac vibrations.

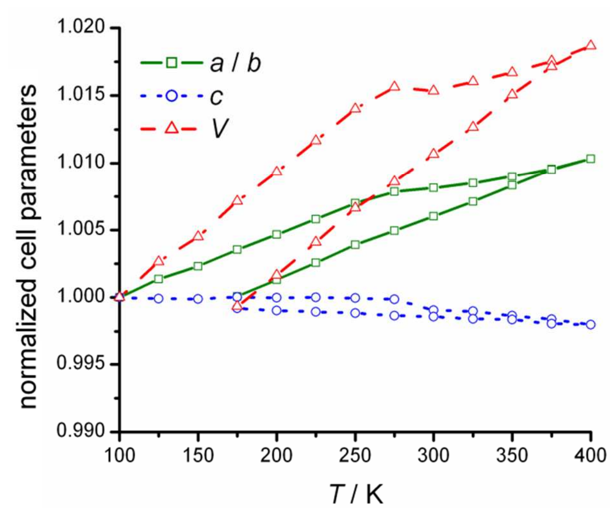

Figure 3. Thermal expansion behaviour in **1**·H_2O → 1 from 100→400→175 K showing PTE in *a* and *V* ZTE in *c*. Cell parameters normalised against the cell of **1**·H_2O at 100 K.

The magnetic susceptibility of a powder sample of **1**·H_2O measured at 0.2 T (figure 4) shows Curie-Weiss behaviour on cooling from 300 K (C = 0.419(2) cm^3Kmol^{-1} and θ = + 26.6(8) K) before a sharp increase with T_C = 9.5 K after which saturation is seen. At 0.004 T, a sharp maximum is seen at 9.3 K. $\chi T(T)$ plots at both fields show increases in value on cooling, indicating ferromagnetic interactions. The magnetisation plot (figure S7, ESI) shows a linear increase in moment with increasing field up to ~0.015 T, after which the gradient increases sharply until saturation is achieved at 0.5 T. This field-dependent switching is characteristic of a metamagnet with the ferromagnetic layers aligning antiferromagnetically with each other below the critical field, H_c and aligning with the external field above H_c, which we see from the magnetisation plot is ~0.01 T. No hysteretic behaviour was seen (figure S8, ESI).

To date, no model exists in the literature for an S = ½ ferromagnetic kagome lattice. Accordingly, we have used exact numerical full-matrix diagonalisation[15] to simulate the behaviour of an n = 12 cluster with periodic boundary conditions (see ESI for full description). From our previous work,[16] we expect this simulation to be accurate at temperatures above 1.2 × $|J/k_B|$ and we have produced a high-temperature series expansion (HTSE) with which to model the behaviour of compound **1**·H_2O:

$$H = -J\sum_{ij} S_i \cdot S_j \quad \text{eq. 1}$$

$$\chi = \frac{Ng^2\mu_B^2}{3k_BT}\cdot S(S+1)\cdot\left(1+\sum_{n=1}^{n=8} a_nK^n\right) \quad \text{eq.2}$$

where $K = J/k_BT$ and a_n values for n = 1−8 are given in the ESI.

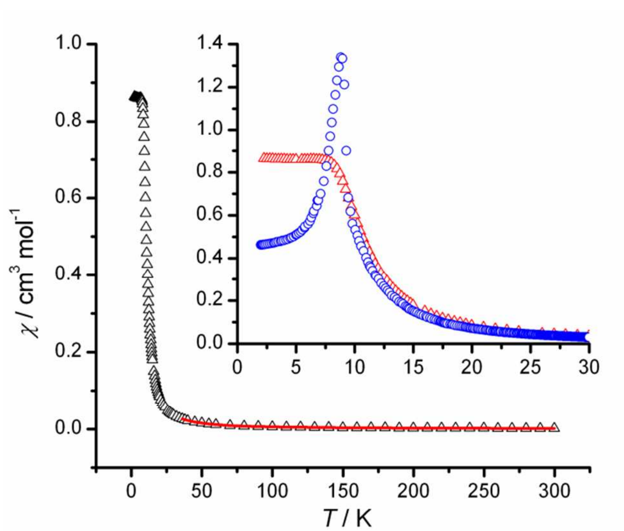

Figure 4. Magnetic susceptibility of **1**·H_2O at 0.2 T with fit from S = ½ ferromagnetic kagome polynomial (solid red line). Inset: magnetic susceptibility at 0.004 T (○) and 0.2 T (Δ).

Using equation 2, we obtain g = 2.100(2) and J/k_B = +31.6(1) K. This coupling indicates that the calculated Curie and Weiss constants are not entirely accurate (usually Curie-Weiss law holds in the temperature range $T > 10 \times J/k_B$), but we include it in this report as an indicator of the overall behaviour to aid in the choice of model. The lack of hysteresis is consistent with the ferromagnetic Heisenberg layer[17] – the small anisotropy giving rise to the orientation of the ferromagnetic moment with respect to the layer plane is of the easy-plane type. The low critical field of the metamagnetic transition arises from the weak dipolar magnetic interaction between the layers over the 13.6066 Å interlayer distance, which is a sufficiently long pathway to negate the effects of superexchange through the bpac ligand.

The kagome lattice in **1**·H_2O is a much sought-after topology in molecular magnetism: because of the hexagonal symmetry of **1**·H_2O, all Cu···Cu interactions are exactly equivalent, simplifying analysis of ferromagnetic behaviour while antiferromagnetic interactions within such a layer would lead to spin frustration and would be an excellent probe in the physics of such phenomena.[18] I the case of a lower-symmetry structure, frustration is usually negated by inequivalent coupling pathways. Two other such $[Cu_3(CO_3)_2]_n^{2n+}$ kagome layers are represented in the literature, [Cu(4-aminopyridine)$_2$ $(CO_3)_2](ClO_4)_2$·½MeOH (**2**)[19] and $[Cu_3(CO_3)_2$(4,4′-bipyridylethane)$_3](ClO_4)_2$ (**3**),[20] neither of which display guest sorption or metamagnetism. A Co(II) kagome built around imdiazole-4,5dicarboxylic acid does show reversible water sorption, but no magnetic data was presented.[21] The magnetic coupling in **2** is slightly under-estimated due to the hexagonal HTSE model and we find that we can reproduce the data well with J/k_B = +12.3(1) K The coupling in **1**·H_2O fits well with the angular dependence found in several $Cu_3(CO_3)$ trimers (Figure S12, ESI) and calculated by Félix *et al.*[22] when only trigonally-symmetric trimers and those close to being ideal in their structure are taken into account. It is worth noting that the couplings in **1**·H_2O and **2** are slightly lower than expected for the Cu−O−C angle, most likely a function of the electronegativity of the coordination sphere: the trimeric clusters used in making this relationship have N_3O_3 or N_4O_2 coordination spheres, pushing more electron density onto the metal centers and allowing a greater orbital overlap between Cu centers, as seen in Cu(oxalate)(L)$_x$ chains.[23] Compound **3** is reported as showing antiferromagnetic couplings in the layer, although the magnetic susceptibility appears to be qualitatively the same as **1**·H_2O and **2**, and antiferromagnetic couplings in this layer type are not consistent with the above angular dependency.

Interestingly, the magnetic properties of **1** are only subtly modified from that of **1**·H_2O (figure S9, ESI), being metamagnetic with a lower T_c of 8.5 K and coupling of +28.3(3) K whereas other hydrated magnets can show more marked switching behaviour on desolvation, such as $[Co_3(OH)_2(C_4O_4)_2]\cdot 3H_2O$ (**4**)[24] and $[Cu_2M(tzdc)_2(H_2O)_2]\cdot 2H_2O$ (M = Fe^{2+} (**5**) or Mn^{2+} (**6**); tzdc = 1,2,3-triazole-4,5-dicarboxylate).[25] In the case of **4**, this switching likely occurs through a very small change to the structure of the metal coupling pathways as there is little difference in the structure on desolvation, whereas in **5** and **6**, a more substantial structural change accompanies the magnetic switching where the layer structure folds to provide an octahedral environment for the Fe and Mn ions after water has been removed from the metals. This highlights the complex nature of magneto-structural correlations in widely-varying structures with varied metal ions in that compound **1** and **4** show similar degrees of structural change on desolvation, yet markedly different magnetic responses. Compound **1** also shows a very low T_c for the metamagnetic transition, especially when compared to other ditopically-bridged layers with shorter diamines.[26]

Conclusions

In compound $\mathbf{1}\cdot H_2O$, we have presented a multifunctional MOF formed by the fixation of CO_2 direct from the air that displays a ferromagnetic kagome lattice, for which we have provided a new magnetic model. The uniaxial ZTE in this compound arises from the transverse vibration of a new type of molecular bridge for this phenomenon and, when coupled to the ease of forming easily-oriented single crystals and stability on desolvation, produces a material of particular interest in relation to precision components requiring precise alignment under varying thermal conditions. Desolvation of $\mathbf{1}\cdot H_2O$ causes only a small modification of the magnitude of the magnetic coupling constant and thermal expansion coefficients, giving a compound that is structurally robust to changes in its host-guest chemistry.

Experimental

Materials and methods

All reagents were purchased from commercial sources and used without further refinement.

A blue hexagonal prism like crystal was attached with vacuum grease on one edge in an open glass capillary inserted in a copper mounting pin. The crystal was quenched in a cold nitrogen gas stream from an Oxford Cryosystems Cryostream. A SuperNova dual source diffractometer with an Atlas CCD employing mirror monochromated MoK_α radiation generated from a SuperNova (Mo) X-ray Source was used for the data collection. Cell constants were obtained from a least squares refinement against 1913 reflections located between 5.9 and 58.8º 2θ. Data were collected at 350(2) Kelvin with ω scans scans to 51.88º 2θ. The data integration and reduction were undertaken with CrysAlisPro,[27] and subsequent computations were carried out with the XP SHELXTL-Plus[28], WinGX[29] and ShelXle[28] graphical user interfaces.

The structure was solved in the space group P6/m (no. 175) by direct methods with SHELXS-97,[28] and extended and refined with SHELXL-97.[28] All of the non-hydrogen atoms were modelled with anisotropic displacement parameters with the exception of the disordered perchlorate atoms. A riding atom model with group displacement parameters was used for the hydrogen atoms. The disordered perchlorate anions were modelled as a rigid body over the symmetry sites.

Variable-temperature single-crystal X-ray diffraction (VT-SCXRD) measurements were performed on the same instrument from 100−400−175 K in 25 increments.

Powder X-ray diffraction patterns were obtained in the 10−50° range using Cu-Kα radiation (λ = 1.5405 Å) on a PANalytical X'Pert Pro MPD in a glass capillary. A Le Bail fit was made to determine phase identity and to identify any impurity contribution, which was not found to be present.

Infrared measurements were performed on a Bruker IFS66V FTIR spectrometer using a single-bounce diamond attenuated total reflectance accessory between 600 and 3400 cm^{-1}. Assignment of bands was made from Nakamoto.[30]

Thermogravimetric measurements were made on a TA Instruments Hi-Res TGA 2950 in the range 21−600 °C in air.

The water adsorption isotherm was measured with a Hiden-Isochema IGA-002 gravimetric system. 60 mg of $\mathbf{1}\cdot H_2O$ was loaded into a mesh basket, and evacuated under high vacuum at 100 °C for 16 hours, after which the sample mass was stable. During measurement of the isotherm the sample was maintained at 25 ± 0.1 °C, while at each pressure point the sample chamber was pressurised to a set pressure of water vapour and allowed to equilibrate for 3 hours before moving to the next pressure point. Void space calculations were made in Mercury CSD 3.1.1 using a probe radius of 1.0 Å.

Magnetic measurements were performed on a Quantum Designs Physical Property Measurement System, (PPMS), with a Vibrating Sample Magnetometer (VSM) attachment. Samples were loaded into a polyethylene sample container and sealed with Teflon tape. Magnetic susceptibility measurements were made on a Quantum Designs PPMS magnetometer from 2−300 K under an applied field of 0.2 T on a 10.25 mg sample. Magnetisation measurements were made between 0−5 T at 2 K. Diamagnetic corrections were made using the equation 0.45 × 10^6 cm^3mol^{-1}.

Synthesis of $[Cu_3(CO_3)_2$(4,4′-bipyridylacetylene)$_3$] $[ClO_4]_2.H_2O$, $\mathbf{1}\cdot H_2O$

Cu(II)$(ClO_4)_2.6H_2O$ (370 mg, 1 mmol) and 4,4′-bipyridylacetylene (180 mg, 1 mmol) were dissolved in 80 ml 15% NH_3 aqueous solution and the solution left exposed to air for two days, after which purple hexagonal crystals of $\mathbf{1}.H_2O$ formed. The crystals were filtered and washed with water and acetone and left to dry. Yield: 319 mg (89 %).

IR (cm^{-1}; attenuated total reflectance; s = strong, m = medium, w = weak, n = narrow, b = broad): 3097 (n, w) C−H stretch; 3054 (n, w) C−H stretch; 1617 (n, m) C=N; 1450 (n, s) and 1430 (n, m) CO_3 ν_3; 1332 (n, w); 1224 (n, m) C−H; 1110 (n, m) and 1083 (n, s) CO_3 ν_1; 1033 (n, m); 870 (n, w); 848 (n, s) and 833 (n, m) CO_3 ν_2; 758 (n,w); 737 (n, w); 623 (n, m).

Elemental analysis (for compound **1**): $C_{38}H_{24}Cl_2Cu_3N_6O_{14}$: expected: C: 43.46; H: 2.30; N: 8.00. Found: 43.54; H: 2.26; N: 7.90.

Acknowledgements

This research was supported by the Australian Research Council (grants DP120101445 and FT100100514), by the Science and Industry Endowment Fund, and by a Marie Curie International Incoming Fellowship (TDK) within the 7th European Community Framework Program (grant PIIF-GA-2011-300462).

Notes and references

[a] Chemistry, University of Southampton, University Road, Highfield, Southampton, SO17 1BJ, UK.

[b] School of Chemistry, The University of Sydney, NSW 2006, Australia.

[c] Australian Synchrotron Company Limited, 800 Blackburn Road, Clayton, Victoria 3168, Australia.

Electronic Supplementary Information (ESI) available: Full characterisation, crystallographic information files (also available free of charge at www.ccdc.cam.ac.uk, CCDC numbers CCDC 931211 for **1**·H_2O and CCDC 931212 for **1**) and a detailed description of the magnetic modelling are provided.. See DOI: 10.1039/b000000x/

1 a) C. J. Kepert, *Metal-Organic Framework Materials* in *Inorganic Materials: Volume One, Porous Materials*, (Eds.: D.W. Bruce, R.I. Walton, D. O'Hare), John Wiley & Sons, Chichester, 2010, pp 1-68; b) L. J. Murray, M. Dincă and J. R. Long, *Chem. Soc. Rev.*, 2009, **38**, 1294-1314; c) S. L. James, *Chem. Soc. Rev.*, 2003, **32**, 276-288.

2 a) P. D. Southon, L. Liu, E. A. Fellows, D. J. Price, G. J. Halder, K. W. Chapman, B. Moubaraki, K. S. Murray, J.-F. Letard and C. J. Kepert, *J. Am. Chem. Soc.*, 2009, **131**, 10998-11009; b) M. Ohba, K. Yoneda, G. Agustí, M. C. Muñoz, A. B. Gaspar, J. A. Real, M. Yamasaki, H. Ando, Y. Nakao, S. Sakaki and S. Kitagawa, *Angew. Chem., Int. Ed.*, 2009, **48**, 4767-4771.

3 a) D. M. D'Alessandro, B Smit, and J. R. Long, *Angew. Chem., Int. Ed.*, 2010, **49**, 6058-6082; b) D. M. D'Alessandro and T. McDonald, *Pure Appl. Chem.*, 2011, **83**, 57-66; c) D. Britt, H. Furukawa, B. Wang, T. G. Glover and O. M. Yaghi, *Proc. Nat. Acad. Sci.*, 2009, **106**, 20637-20640.

4 a) B. Metz, O. Davidson, H. de Coninck, M. Loos, and L. Meyer, *IPCC Special Report on Carbon Dioxide Capture and Storage*, Cambridge University Press, UK, 2005; b) G. T. Rochelle, *Science*, 2009, **325**, 1652-1654; c) R. S. Haszeldine, *Science*, 2009, **325**, 1647-1652; d) K. Z. House, C. F. Harvey, M. J. Aziz and D. P. Schrag, *Energy Environ. Sci.*, 2009, **2**, 193-205; e) P. D. Vaidya and E. Y. Kenig, *Chem. Eng. Technol.*, 2007, **30**, 1467-1474.

5 a) A. Demessence, D. M. D'Alessandro, M. L. Foo and J. R. Long, *J. Am. Chem. Soc.*, 2009, **131**, 8784-8786; b) S. Choi, T. Watanabe, T.-H. Bae, D. S. Sholl, and C. W. Jones, *J. Chem. Phys. Lett.*, 2012, **3**, 1136-1141.

6 a) D. M. Kiefer, *Today's Chemist at Work*, 2002, **11**, 87-88; b) K. S. Lackner, *Annu. Rev. Energy Environ.*, 2002, **27**, 193-232.

7 a) E. A. Quadrelli, G. Centi, J.-L. Duplan and S. Perathoner, *ChemSusChem*, 2011, **4**, 1194-1215; b) M. Peters, B. Köhler, W. Kuckshinrichs, W. Leitner, P. Markewitz and T. E. Müller, *ChemSusChem,* 2011, **4**, 1216-1240.

8 A. L. Goodwin and C. J. Kepert, *Phys. Rev. B*, 2005, **71**, 140301.

9 See for example: a) S. G. Duyker, V. K. Peterson, G. J. Kearley, A. J. Ramirez-Cuesta and C. J. Kepert, *Angew. Chem., Int. Ed.*, 2013, **52**, 5266-5270; b) A. L. Goodwin, M. Calleja, M. J. Conterio, M. T. Dove, J. S. O. Evans, D. A. Keen, L. Peters and M. G. Tucker, *Science*, 2008, **319**, 794-797; c) A. L. Goodwin, B. J. Kennedy, and C. J. Kepert, *J. Am. Chem. Soc.*, 2009, **131**, 6334-6335; d) A. E. Phillips, A. L. Goodwin, G. J. Halder, P. D. Southon and C. J. Kepert, *Angew. Chem., Int. Ed.* 2008, **47**, 1396-1399,

10 See for example: a) N. Lock, M. Christensen, C. J. Kepert and B. B. Iversen, *Chem. Commun.*, 2013, **49**, 789-791; b) N. Lock, Y. Wu, M. Christensen, L. J. Cameron, V. K. Peterson, A. J. Bridgeman, C. J. Kepert and B. B. Iversen, *J. Phys. Chem. C*, 2010, **114**, 16181-16186; c) V. K. Peterson, G. J. Kearley, Y. Wu, A. J. Ramirez-Cuesta, E. Kemner and C. J. Kepert, *Angew. Chem., Int. Ed.*, 2010, **49**, 585-588; d) Y. Wu, A. Kobayashi, G. J. Halder, V. K. Peterson, K. W. Chapman, N. Lock, P. D. Southon and C. J. Kepert, *Angew. Chem., Int. Ed.*, 2008, **47**, 8929-8932; e) Y.-S. Wei, K.-J. Chen, P.-Q. Liao, B.-Y. Zhu, R.-B. Lin, H.-L. Zhou, B.-Y. Wang, W. Xue, J.-P. Zhang and X.-M. Chen, *Chem. Sci.*, 2013, **4**, 1539-1546.

11 a) T. D. Keene, D. Rankine, J. D. Evans, P. D. Southon, C. J. Kepert, J. B. Aitken, C. J. Sumby and C. J. Doonan, *Dalton Trans.*, 2013, **42**, 7871-7879; b) P. Dechambenoit, and J. R. Long, *Chem. Soc. Rev.*, 2011, **40**, 3249-3265; c) M. Kurmoo, *Chem. Soc. Rev.*, 2009, **38**, 1353-1379.

12 Crystal data for **1**·H_2O: $C_{38}H_{26}Cl_2Cu_3N_6O_{15}$, 1068.16 gmol^{-1}, hexagonal $P6/m$ (no. 165), 150 K, a = b = 9.2000(2) Å, c = 13.6033(3) Å, V = 997.13(4) Å^3, Z = 1, ρ_{calc} = 1.775 gcm^{-1}, μ = 1.800 mm^{-1}, λ = 0.71073 Å (Mo-Kα), $2\theta_{max}$ = 25.98°, 9572 reflections measured (692 unique, R_{int} = 0.0224), R_1 / wR_2 (I > 2σ) = 0.0364 / 0.1090 (672 reflections), R_1 / wR_2 (all data) = 0.0372 / 0.1096 (692 reflections), residual electron density: max = 0.612 e$^-$Å^3, min = −0.539 e$^-$Å^3, rms = 0.083 e$^-$Å^3.

13 Crystal data for **1**: $C_{38}H_{24}Cl_2Cu_3N_6O_{14}$, 1050.16 gmol^{-1}, hexagonal $P6/m$ (no. 165), 350 K, a = b = 9.2577(3) Å, c = 13.5853(5) Å, V = 1008.33(6) Å^3, Z = 1, ρ_{calc} = 1.729 gcm^{-1}, μ = 1.777 mm^{-1}, λ = 0.71073 Å (Mo-Kα), $2\theta_{max}$ = 25.98°, 5479 reflections measured (701 unique, R_{int} = 0.0298), R_1 / wR_2 (I > 2σ) = 0.0347 / 0.0988 (582 reflections), R_1 / wR_2 (all data) = 0.0453 / 0.1071 (701 reflections), residual electron density: max = 0.695 e$^-$Å^3, min = −0.436 e$^-$Å^3, rms = 0.073 e$^-$Å^3.

14 a) A. L. Goodwin, K. W. Chapman and C. J. Kepert, *J. Am. Chem. Soc.*, 2005, **127**, 17980-17981; b) A. E. Phillips, G. J. Halder, K. W. Chapman, A. L. Goodwin and C. J. Kepert, *J. Am. Chem. Soc.*, 2010, **132**, 10-11.

15 a) O. Waldmann, *Phys. Rev. B*, 2000, **61**, 6138-6144; b) O. Waldmann, H. U. Güdel, T. L. Kelly and L. K. Thompson, *Inorg. Chem.*, 2006, **45**, 3295-3300.

16 T. D. Keene, Y.-H. Deng, F.-G. Li, Y.-F. Ding, B. Wu, S.-X. Liu, C. Ambrus, O. Waldmann, S. Decurtin and X.-J. Yang, *Inorg. Chim. Acta*, 2009, **362**, 2265-2269.

17 See for example J. G. DaSilva and J. S. Miller, *Dalton Trans.*, 2013, **42**, 8334-8338.

18 See for example: a) A. Harrison, *J. Phys.: Condens. Matter*, 2004, **16**, S553; b) S. Yan, D. A. Huse and S. R. White, *Science*, 2011, **332**, 1173-1176; c) M. V. Gvozdikova, P. E. Melchy and M. E. Zhitomirsky, *J. Phys.: Condens. Matter*, 2011, **23**, 164209.

19 A. Majumder, C. R. Choudhury, S. Mitra, G. A. Rosair, M. S. El Fallah, and J. Ribas, *Chem. Commun.*, 2005, 2158-2160.

20 P. Kanoo, C. Madhu, G. Mostafa, T. K. Maji, A. Sundaresan, S. K. Pati and C. N. R. Rao, *Dalton Trans.*, 2009, 5062-5064.

21 C.-J. Li, S. Hu, W. Li, C.-K. Lam, Y.-Z. Zheng and M.-L. Tong, *Eur. J. Inorg. Chem.*, 2006, 1931-1935.

22 P. Mateus, R. Delgado, F. Lloret, J. Cano, P. Brandão and V. Félix, *Chem. Eur. J.*, 2011, **17**, 11193-11203.

23 U. García-Couceiro, O. Castillo, A. Luque. J. P. García-Terán, G. Beobide and P Román, *Cryst. Growth Des.*, 2006, **6**, 1839-1847.

24 a) M. Kurmoo, H. Kumagai, K. W. Chapman and C. J. Kepert, *Chem. Commun.*, 2005, 3012-3014. b) R. A. Mole, J. A. Stride, P. F. Henry, M. Hoelzel, A. Senyshyn, A. Alberola, C. J. Gómez Garcia, P. R. Raithby and P. T. Wood, *Inorg. Chem.*, 2011, **50**, 2246-2251.

25 W.-X. Zhang, W. Xue, and X.-M. Chen, *Inorg. Chem.*, 2011, **50**, 309-3016.

26 See for example: T. D. Keene, M. E. Light, M. B. Hursthouse, and D. J. Price, *Dalton Trans.*, 2011, **40**, 2983-2994.

27 *CrysAlisPro*, Agilent Technologies XRD Products, Yarnton, Oxfordshire. OX5 1QU, UK.

28 G. M. Sheldrick, *Acta Crystallogr.*, 2008, **D64**, 112-122.

29 L. J. Farrugia, *WinGX*, *J. Appl. Cryst.*, 1999, **32**, 837-838.

30 K. Nakamoto, *Infrared and Raman Spectra of Inorganic and Coordination Compounds, Part A, Theory and Applications in Inorganic Chemistry, 6th Edition*, JohnWiley & Sons, Inc.,Hoboken, 2009.

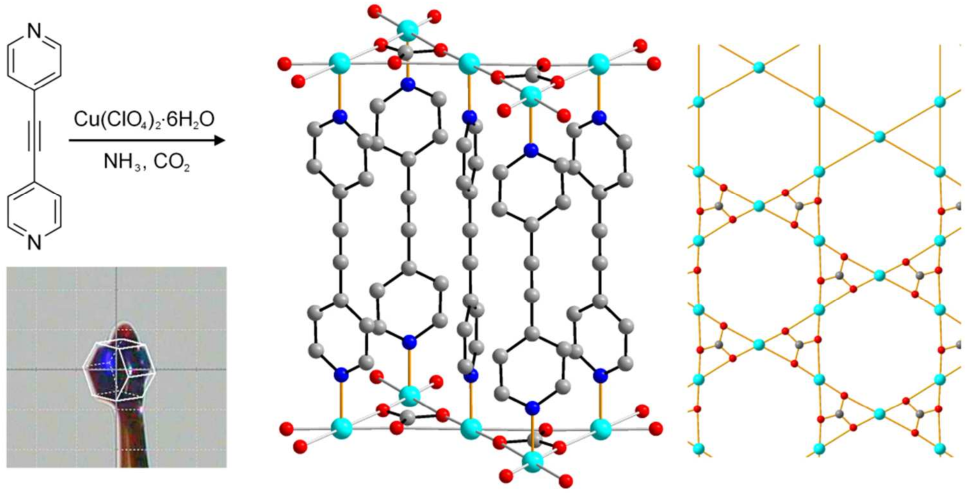

91x48mm (300 x 300 DPI)